STELLAR AND GAS DYNAMICS OF MERGING GALAXIES

Joshua E. Barnes
Canadian Institute for Theoretical Astrophysics
60 Saint George St., Toronto, Ontario, M5S 1A1
CANADA

ABSTRACT. Numerical models permit a detailed study of the dynamics of merging disk galaxies. To first order, a typical galactic encounter is a well-posed problem in collisionless stellar-dynamics, since $\gtrsim 90\%$ of the mass is in the form of stars or dark matter. Mergers between disk/halo galaxies produce objects resembling elliptical galaxies in structure and kinematics. The three major orbit families expected in triaxial ellipsoids are all present in these merger remnants, and the distribution of stars between orbit families reflects the initial orientations of the colliding disks.

Models including gas dynamics, developed in collaboration with L. Hernquist, show how mergers, and perhaps other violent interactions, may fuel nuclear starbursts. In these experiments a large fraction ($\sim 60\%$) of the gas distributed throughout the galactic disks winds up in a central cloud with dimensions of a few hundred parsecs, a result of gravitational torques which transfer angular momentum from the gas to stellar bar. Nuclear gas clouds and starbursts observed in merging galaxies such as NGC 520 and Arp 220 may well be generated by this mechanism.

1. Introduction

Mergers of fully formed disk galaxies have recently attracted much attention as a plausible formation mechanism for many kinds of active galaxies. This interest stems from observations implicating mergers in the origins of infrared-luminous galaxies (Joseph & Wright 1985, Sanders *et al.* 1988), powerful radio galaxies (Heckman *et al.* 1986), and quasars (*cf.* Stockton 1990). Another line of inquiry, originally motivated largely by theoretical issues, has focused on mergers as a formation mechanism for elliptical galaxies (Toomre & Toomre 1972). The possible connections between these two lines of investigation have not been extensively explored.

Self-consistent numerical simulations of galactic mergers are at the point where accurate model results can be obtained. Much of this work has been reviewed by Barnes (1990). This paper will concentrate on two new developments. The first concerns the orbit structure of disk merger remnants. The second is the inclusion of gas dynamics in merger simulations.

2. Merger Experiments

Modeling the collision and merger of a pair of disk galaxies is relatively straightforward as long as only collisionless components (*i.e.* stars and dark matter) are included. The main demand which must be met by a faithful simulation is particle number. Roughly 10^4 particles are needed to model a self-gravitating disk galaxy; with fewer particles, swing amplification (*e.g.* Toomre 1981) of $\sqrt{N}$ fluctuations produces perturbations which rapidly

F. Combes and F. Casoli (eds.), Dynamics of Galaxies and Their Molecular Cloud Distributions, 363–372.
© 1991 *IAU. Printed in the Netherlands.*

https://doi.org/10.1017/S0074180900244562 Published online by Cambridge University Press

degrade the structure of the model. To model collisions between disk galaxies with fairly realistic structure, however, requires a three-dimensional N-body code capable of high resolution. Grid-based codes are at a disadvantage here because the grid limits the resolution. Older studies (*e.g.* Gerhard 1981, Farouki & Shapiro 1982, Negroponte & White 1983) used direct-summation codes to obtain high resolution. Hierarchical methods (*e.g.* Barnes & Hut 1986, Greengard 1990) now provide comparable resolution at a cost scaling with particle number N of only $O(N \log N)$ instead of $O(N^2)$. In practice, research-grade calculations require a supercomputer or a very fast workstation, but the results obtained can well justify the resources needed.

Considerable effort is also required to develop reasonably stable models of disk galaxies to use in such calculations. The experiments described here employ composite models, each consisting of a central spheroidal bulge, thin exponential disk, and extended dark halo, with mass ratios of 1:3:16 respectively. All three components are modeled as fully self-consistent N-body systems; each galaxy contains 2048 bulge, 6144 disk, and 8192 halo particles. The set-up procedure is described by Barnes (1988). In these calculations I use an arbitrary system of units with $G \equiv 1$. Each galaxy has a total mass of 1.25 and a binding energy of -1.38; the disks have exponential scale lengths of $\alpha^{-1} = 1/12$ and rotate once every 0.93 time units at a radius of $3/\alpha$. Crudely scaling one of these disks to the Milky Way, the units of length, time, and mass become 40 kpc, 250 Myr, and 2.2×10^{11} $M_\odot$, respectively.

Figure 1 shows two projections of a typical merger remnant. This object was derived from a close parabolic collision of two disk/halo galaxies. Parameters for this and a few other collision experiments are listed in Table 1. These particular examples were selected from an ensemble of about a dozen to illustrate different kinds of remnant structures.

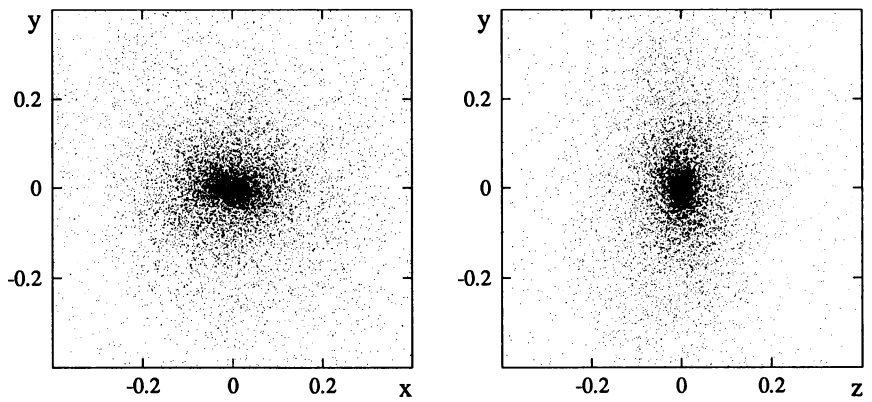

Figure 1. Outcome of a parabolic collision and merger of two disk/halo galaxies, encounter 1 from Table 1. Only the luminous particles are plotted. Here x, y, and z are the major, intermediate, and minor axes of the remnant, respectively.

In general, mergers of bulge/disk/halo galaxies produce triaxial ellipsoids with many of the properties of elliptical galaxies (Barnes 1988, 1990). Merging only partly scrambles the initial ordering of particles in binding energy (White 1979), so the remnants are dominated by particles from the bulges at small radii, from the bulges and disks combined at intermediate radii, and from the halos at larger radii. However, the merging process is sufficiently tumultuous to set up a projected "luminosity profile" derived from the bulge

https://doi.org/10.1017/S0074180900244562 Published online by Cambridge University Press

Table 1. Parameters for parabolic disk-galaxy collisions. R_p is the pericentric separation; the orientation of each disk is specified by the inclination i and pericentric argument ω, following Toomre & Toomre (1972).

No.	R_p	i_1	ω_1	i_2	ω_2
1	0.4	71	30	0	
2	0.4	180		109	30
3	0.2	71	90	109	90

and disk particles closely approximating a de Vaucouleurs law; such a profile seems to be a generic result of violent relaxation (van Albada 1982). Much of the orbital energy of the two galaxies is transferred to the dark halo component as the galaxies merge. As a result, the luminous components are rather tightly bound, with projected half-light radii r_e only slightly larger than the exponential scale lengths of the original disks, and central velocity dispersions a factor of ~ 1.4 times the value expected from homology arguments (Hausman & Ostriker 1978, White 1983). The dark halo also absorbs much of the angular momentum, leaving the remnant with kinematical properties typical of bright, slowly-rotating elliptical galaxies.

3. Orbit Analysis

Orbit analysis provides a way to "deconstruct" merger remnants and thereby gain a more detailed understanding of their dynamics. This work is rather new, and the method is still under development; it is not yet clear how far the results can be trusted. As van Albada (1987) has emphasized, orbits in N-body simulations are subject to perturbations due to fluctuations in the potential. Nonetheless the results given here are fairly robust and reproducible from one calculation to another.

3.1. METHOD

The analysis begins with a remnant run far enough past merger that the mass distribution has reached an approximate equilibrium. First one defines a coordinate system x, y, z aligned with the remnant major, intermediate, and minor axes, respectively. The gravitational potential is computed next; since these remnants are close to a triaxial ellipsoid in shape, I chose to represent the field in cartesian moments (*e.g.* Hernquist & Barnes 1990), retaining only the monopole and quadrupole components of the expansion (the dipole vanishes by symmetry). These moments are tabulated on a radial grid, and interpolation is used to obtain the potential and force at any point $\mathbf{r} \equiv (x, y, z)$.

To classify the orbit of a particle, I follow its motion in the model potential for a number of orbital periods, watching for sign changes in the components of the angular momentum $\mathbf{r} \times \dot{\mathbf{r}} = \mathbf{j} = (j_x, j_y, j_z)$. In a spherical potential, of course, $\mathbf{j}$ is conserved, while in a general potential any or all of the components of $\mathbf{j}$ may change sign. Define k_i to be 1 if j_i does *not* change sign, 0 if it does, where i is x, y, or z. The quantity $k \equiv k_x + 2k_y + 4k_z$, which can take on $2^3 = 8$ possible values, gives the desired classification of the orbit.

In a typical triaxial potential, only three of the eight possible values of k correspond to stable orbits (*e.g.* Schwarzschild 1979, de Zeeuw 1985). The three main orbit families are:

1. Box orbits; $k = 0$. All three components of $\mathbf{j}$ change sign; the orbit fills out a box-shaped region passing through the center.

https://doi.org/10.1017/S0074180900244562 Published online by Cambridge University Press

2. X-tube orbits; $k = 1$. Here j_y and j_z change sign while j_x does not; the orbit loops around the x axis without changing direction.
3. Z-tube orbits; $k = 4$. Here j_x and j_y change sign while j_z does not; the orbit loops around the z axis.

When the classification procedure above is applied to the merger remnants generated in N-body simulations, 95% or more of the particle orbits typically belong to one of these three main families. This may be taken as further evidence that the remnant potentials are approximately triaxial. It also provides a welcome consistency check for the procedure.

3.2. RESULTS

The remnant produced by encounter 1 has a relatively simple structure which is nicely elucidated by orbit analysis. In this encounter, the angular momentum vector of one disk was precisely parallel to the orbital angular momentum, while the other disk was tipped at an inclination of 71°. Both galaxies thus experienced prograde encounters and responded by flinging out long tidal tails before merging. The final encounter of the two central bulges produced a slightly elongated central region surrounded by material from the disks of the two victims.

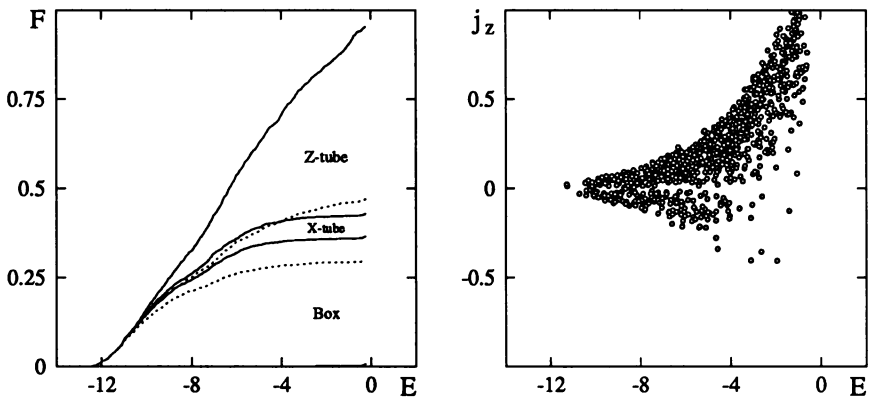

Figure 2. *Left:* Cumulative distribution of orbit class for luminous particles in remnant 1, plotted as a function of binding energy. *Right:* z-component of angular momentum *vs.* binding energy for the Z-tube orbits.

Figure 2 shows the cumulative distribution of orbit class as a function of specific binding energy E for a sample of 2048 luminous particles from this remnant (solid lines). The most tightly bound particles are almost all on box orbits, helping to support the triaxial shape of the central region. Further out, the remnant is dominated by particles on Z-tube orbits. The vast majority of these tubes orbit the remnant in the same direction as the two galaxies originally orbited each other; these tubes give the outer part of this remnant the predominantly oblate shape seen in Figure 1. This object is significantly flattened by rotation at large radii; the rotation is a "relic" of the spins of the original disks.

The dotted lines in Figure 2 show the result of applying the orbit classification procedure to a isotropic test distribution with the same $f(E)$ as the luminous sample[1]. The purpose of this exercise is to measure the phase-space volume available to each orbital family in

[1] Indeed, this test distribution was constructed from the luminous sample by iterating the following

https://doi.org/10.1017/S0074180900244562 Published online by Cambridge University Press

the model potential. In this case the available phase-space volume in this potential is also dominated by the Z-tube family. X-tube orbits are roughly half as common in the actual remnant as they are in the isotropic sample.

Simply reversing the spins of both disk, as in encounter 2, produces a very different result. This collision is somewhat less dramatic since the disks do not develop such impressive tidal tails in a retrograde passage. This remnant is nearly oblate at the center and becomes more triaxial at larger radii. As Figure 3 shows, it has a much larger population of box orbits than the previous example. The large number of boxes is in part a reflection of the triaxial form of the remnant. This object is strikingly deficient in X-tube orbits, as one can see by comparing the solid and dotted curves.

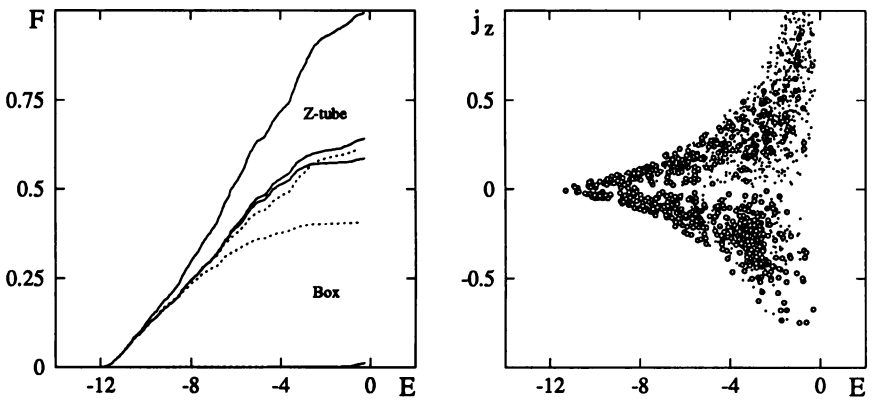

Figure 3. *Left:* Orbit class *vs.* binding energy for remnant 2. *Right:* j_z plotted against E for Z-tube orbits. Circles are luminous particles, points are halo particles.

The most remarkable property of this remnant is shown in the right-hand panel of Figure 3. Here results are presented for the halo (points) as well as the luminous component (circles). Most halo Z-tube orbits have $j_z > 0$, a relic of the orbital angular momentum of the two galaxies. The luminous Z-tube orbits, however, tend to circle the remnant in the *opposite* direction, reflecting the spins of the disks they came from. Such counter-streaming of different populations is a distinctive signature of the merging process.

Results for encounter 3 are presented in Figure 4. In this case both disks are inclined; in fact, both lie in the same plane, tilted by 71° from the orbit, but spin in opposite directions. This encounter is considerably closer than the previous two examples, and the galaxies merge more rapidly. The resulting remnant is triaxial at small radii but becomes more nearly prolate further out. This object has a large population of X-tube orbits. The right-hand panel of Figure 4 shows how the opposing spins of the two original disks have left their mark on the remnant; particles from one disk tend to have $j_x > 0$, while those from the other move the opposite way. These two sub-populations largely cancel each others

procedure: first, randomize the direction of the velocity vector of each particle in the sample, leaving the magnitude unchanged; second, follow the motion of each particle in the model potential for a few orbits. This process leaves $f(E)$ unchanged but erases any other structure the distribution may have. After several iterations the distribution converges on a unique limit as judged from the results of orbit classification.

https://doi.org/10.1017/S0074180900244562 Published online by Cambridge University Press

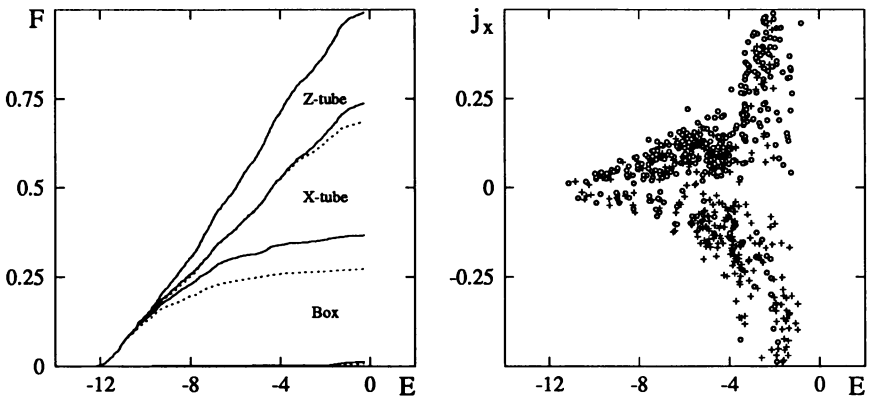

Figure 4. *Left:* Orbit class *vs.* binding energy for remnant 3. *Right:* j_x plotted against E for X-tube orbits. Circles are luminous particles from galaxy one, crosses from galaxy two.

angular momentum; had the initial spin of one of the two disks been reversed, however, the resulting remnant would probably exhibit significant minor axis rotation.

4. Mergers with Gas Dynamics

Compared to purely stellar-dynamical models, simulations including gas dynamics are still in their infancy. The real challenge, which we are far from meeting, is to capture the multi-phase structure of the interstellar medium. Early simulations by Negroponte & White (1983) used "sticky particle" methods in which particles representing the gas bounce off each other with a coefficient of restitution less than unity. This procedure incorporates the effects of dissipation without attempting to model the actual gas dynamics in any detail. The model described in this section, developed in collaboration with L. Hernquist, employs a more ambitious technique known as "smoothed particle" hydrodynamics or SPH (*e.g.* Monaghan 1985). In this method, particles representing fluid elements respond to forces due to pressure as well as gravity; pressure gradients are estimated by averaging the contribution of each gas particle over a region a few times the interparticle spacing. In principle, SPH can accurately model the hydrodynamics and thermodynamics of reasonably smooth gas flows; artificial viscosity is included to deal with shocks. The code used for these simulations is fully described by Hernquist & Katz (1989).

A single experiment, using a total of 90112 particles, is presented in Figure 5; only the 16384 gas particles are shown in the large, unframed plots. This collision is a closer ($R_p = 0.2$) version of encounter 1. The gas is initially distributed just like the disk particles, and amounts to 10% of the disk mass. For further details of this simulation see Barnes & Hernquist (1990).

The overall behavior of this system is very similar to that observed in purely stellar-dynamical models; the two galaxies fly past each other, launch extended tidal tails, fall back together, and rather quickly merge. On large scales the gas and disk stars have similar distributions, although both the spirals due to swing-amplified $\sqrt{N}$ noise at $t = 0.5$ and the narrow tidal features at $t = 1.25$ are more crisply defined by the gas. On small scales, however, the gas and stars develop remarkably different distributions. Some of these

https://doi.org/10.1017/S0074180900244562 Published online by Cambridge University Press

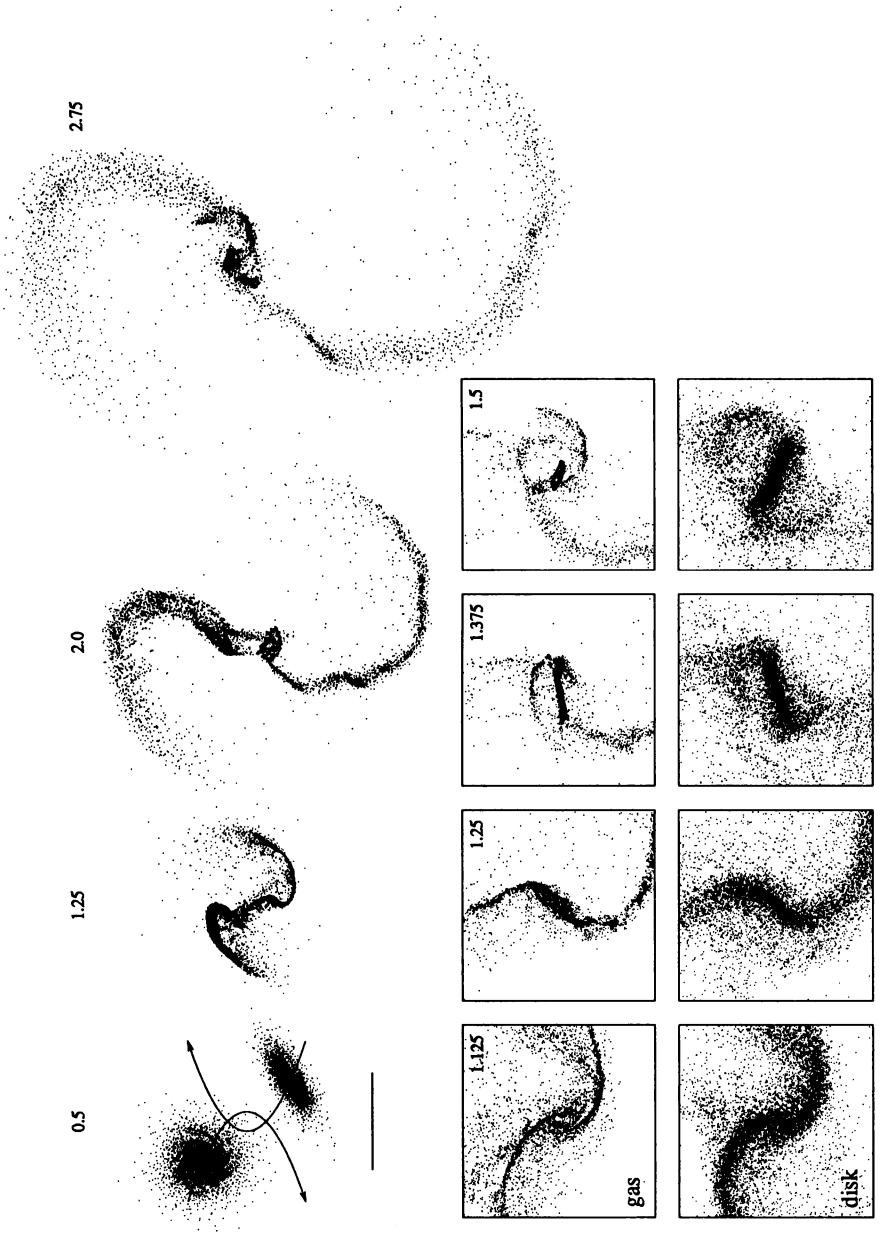

Figure 5. Close encounter and merger of two gas-rich disk galaxies, viewed face-on to the orbital plane. The unframed plots show the *gas* distribution only. The first of these also shows the parabolic trajectories of the two incoming disks; the solid line underneath is one unit of length (40 kpc). Numbers give elapsed time, with pericenter at $t = 1$ (250 Myr). The two rows of smaller plots are 5× enlargements showing the behavior of the gas (top) and disk stars (bottom) in the face-on ($i = 0$) disk.

https://doi.org/10.1017/S0074180900244562 Published online by Cambridge University Press

differences are illustrated in the two rows of small framed plots, which compare the gas and disk stars in the central region of the $i = 0$ disk. As in other collisionless calculations (*e.g.* Noguchi 1987, Barnes 1988, Gerin *et al.* 1990) this disk develops a very pronounced bar as a result of the strong tidal field it has been subjected to. The gas initially responds in a similar fashion, but even in the first small frame narrow features representing high Mach-number shocks are seen. In later frames the gas bar first becomes narrower, and then shrinks in length as well. A surprising amount of material – over half the gas in the disk – is concentrated in the dense oval ring seen in the last small frame. The other disk exhibits similar behavior, despite its 71° inclination.

Rapid inflows of gas have been reported in a number of simulations of barred galaxies. There is some uncertainty, however, concerning the mechanism responsible. According to Simkin *et al.* (1980) and Schwarz (1984) an Inner Linblad Resonance is necessary for rapid inflow. On the other hand, Noguchi (1988) suggested that the bar's strength, rather than its pattern speed, was the key ingredient, and Combes & Gerin (1985) reported that when an ILR is present the gas collects in an inner ring instead of flowing all the way to the center. No ILR exists in the simulation presented here; the pattern speed is slightly greater than the peak value of $\Omega - \kappa/2$, and gas particles populate only the X_1 orbital family (van Albada & Sanders 1982) parallel to the bar.

By measuring the forces on the gas, it is possible to show that the torques responsible for this inflow are *gravitational*; hydrodynamic torques play no significant role in driving the gas to the center (*e.g.* Combes, Dupraz, & Gerin 1990, Barnes & Hernquist 1990). The physics of this situation appears similar to that of an accretion disk with tidally induced spiral shock waves (*e.g.* Spruit 1990). There, the wave deposits negative angular momentum in the disk as it dissipates, driving the accretion flow; this angular momentum is lost to the object generating the tidal field. Here, the gravitational field of the bar sets up a very strong shock in the gas flow; as a result, the gas moves inward, and its angular momentum is transferred back to the bar. The crucial feature seems to be the shocks, which introduce a irreversible aspect to the evolution of the system. We found that inflow could be shut off by disabling radiative cooling; instead of rapidly cooling to $\sim 10^4$ K (where we placed a floor on the cooling function) the gas is shock-heated to $\gtrsim 10^6$ K and forms an extended cloud around the center of the galaxy. Strong radiative shocks thus appear necessary for the bar to drive a rapid inflow of gas.

When the two galaxies merge, both disks contain compact, rapidly spinning rings accounting for more than half of all the gas in the system. These gas rings meet nearly head-on and coalesce, canceling some of their angular momentum when they do. The resulting object, which might be described as an irregular, lumpy cloud of gas, loses additional angular momentum through gravitational torques (*i.e.* dynamical friction). Thus by the end of this experiment, some two rotation periods after the galaxies first encountered each other, $\sim 60\%$ of all the gas in the system is found within a radius of 0.005. Rephrased in dimensional units, this corresponds to $\sim 5 \times 10^9$ $M_\odot$ within ~ 200 pc. Figure 6 compares the distribution of stars and gas in the merger remnant. The stars have rather smooth and regular distribution, in marked contrast to the gas. Indeed, the stellar distribution is quite similar to that seen in near-IR images of Arp 220 which disclose an older population with a de Vaucouleurs' profile (Wright *et al.* 1990). The effective radius of this remnant is 0.1 length units, corresponding to ~ 4 kpc.

https://doi.org/10.1017/S0074180900244562 Published online by Cambridge University Press

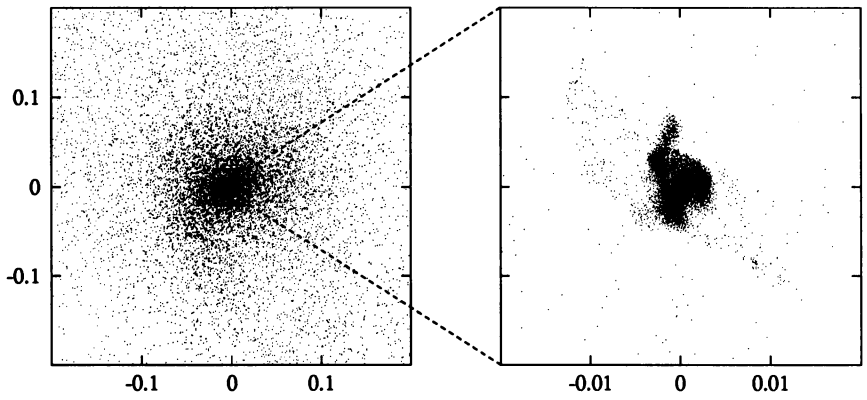

Figure 6. *Left:* luminous particles in the remnant produced by the merger shown in Figure 5, projected onto the orbital plane. *Right:* a 10× enlargement showing the nuclear gas cloud.

5. Discussion

The gas-dynamical calculations presented in the last section suggest a plausible mechanism for fueling nuclear starbursts in strongly interacting disk galaxies and their merger remnants. Similar nuclear inflows have been found in simulations of mergers (Negroponte & White 1983), satellite accretion (Hernquist 1989), and even passing encounters (Noguchi 1988, also these proceedings). The main uncertainties in these calculations concern rapid star formation, which could deplete or disperse the gas before it attained the high densities seen in these simulations. However, the remarkably dense molecular cores found in ultraluminous IRAS galaxies (*e.g.* Sanders, these proceedings) may be taken as evidence that significant amounts of gas accumulate despite rapid star formation. It is not clear what mechanisms might permit some of the gas to continue losing angular momentum and collapse to the much smaller scales where it could fuel an AGN; beyond the tidal braking described here, fragmentation and instabilities in a self-gravitating gas cloud may play an important role (*e.g.* Begelman *et al.* 1984, Norman & Scoville 1988, Shlosman *et al.* 1989).

After star formation, nuclear activity, and outflows have consumed the gas, the resulting remnants should have many of the characteristics of elliptical galaxies. Such relics will exhibit diverse kinematics (*e.g.* Franx *et al.* 1989) reflecting the wide range of possible encounter geometries. By comparing different tracers such as globular clusters and planetary nebulae and by detailed studies of line profiles (*e.g.* Bender 1990), we may be able to identify ellipticals which are products of simple disk-galaxy mergers (as opposed, for example, to ellipticals produced by multiple mergers in compact groups (*e.g.* Barnes 1989)). Star formation in central gas clouds could leave behind a metal-rich population with distinct kinematics (Franx & Illingworth 1988) and higher phase-space densities than those attained by the stellar components of the original galaxies. The starbursts observed in merging systems would then be low-redshift analogs of galaxy transformation at higher redshifts. If so, and if such mergers can indeed trigger nuclear activity (*e.g.* Scoville, these proceedings) the broad peak of QSO activity at redshifts $z \simeq 2$ to 3 may signal the formation of the majority of cluster ellipticals.

https://doi.org/10.1017/S0074180900244562 Published online by Cambridge University Press

It is a pleasure to thank Lars Hernquist for permission to present results from our work in advance of publication. I also wish to thank Marijn Franx for discussions on orbit structure, and Scott Tremaine for discussions on gas dynamics.

Barnes, J.E. 1988. *Ap. J.* 331:699
Barnes, J.E. 1989. *Nature* 338:132
Barnes, J.E. 1990. in *Dynamics and Interactions of Galaxies*, ed. R. Wielen (Berlin: Springer-Verlag), p. 186
Barnes, J.E., Hernquist, L. *Ap. J. Lett.* submitted
Barnes, J.E., Hut, P. 1986. *Nature* 324:446
Begelman, M.C., Blanford, R.D., Rees, M.J. 1984. *Rev. Mod. Phys.* 56:255
Bender, R. 1990. *Astron. Astrophys.* 229:441
Combes, F., Gerin, M. 1985. *Astron. Astrophys.* 150:327
Combes, F., Dupraz, C., Gerin, M. 1990. in *Dynamics and Interactions of Galaxies*, ed. R. Wielen (Berlin: Springer-Verlag), p. 205
de Zeeuw, P.T. 1985. *MNRAS* 216:273
Farouki, R.T., Shapiro, S.L. 1982. *Ap. J.* 259:103
Franx, M., Illingworth, G.D. 1988. *Ap. J.* 327:L55
Franx, M., Illingworth, G., Heckman, T. 1989. *Ap. J.* 344:613
Gerhard, O.E. 1981. *MNRAS* 197:179
Gerin, M., Combes, F., Athanassoula, A. 1990. *Astron. Astrophys.* 230:37
Greengard, L. 1990. *Computers in Physics* 4:142
Hausman, M., Ostriker, J. 1978. *Ap. J.* 224:320
Heckman, T.M., Smith, E.P., Baum, S.A., van Breugel, W.J.M., Miley, G.K., Illingworth, G.D., Bothun, G.D., Balick, B. 1986. *Ap. J.* 311:526
Hernquist, L. 1989. *Nature* 340:687
Hernquist, L., Barnes, J.E. 1990. *Ap. J.* 349:562
Hernquist, L., Katz, N. 1989. *Ap. J. Suppl.* 70:419
Joseph, R.D., Wright, G.S. 1985. *MNRAS* 214:87
Monaghan, J. 1985. *Comp. Phys. Rep.* 3:71
Negroponte, J., White, S.D.M. 1983. *MNRAS* 205:1009
Noguchi, M. 1987. *MNRAS* 228:635
Noguchi, M. 1988. *Astron. Astrophys.* 203:259
Norman, C., Scoville, N.Z. 1988. *Ap. J.* 332:124
Sanders, D.B., Soifer, B.T., Elias, J.H., Madore, B.F., Matthews, K., Neugebauer, G., Scoville, N.Z. 1988. *Ap. J.* 325:74
Schwarz, M.P. 1984. *MNRAS* 209:93
Schwarzschild, M. 1979. *Ap. J.* 232:236
Shlosman, I., Frank, J., Begelman, M.C. 1989. *Nature* 338:45
Simkin, S.M., Su, H.J., Schwarz, M.P. 1980. *Ap. J.* 237:404
Spruit, H.C. 1990. in *Theory of Accretion Disks*, eds. F. Meyer, W.J. Duschl, J. Frank, E. Meyer-Hofmeister (Dordrecht: Kluwer), p. 325
Stockton, A. 1990. in *Dynamics and Interactions of Galaxies*, ed. R. Wielen (Berlin: Springer-Verlag), p. 440
Toomre, A. 1981. in *The Structure and Evolution of Normal Galaxies*, eds. S.M. Fall & D. Lynden-Bell (Cambridge: Cambridge Univ. Press), p. 111
Toomre, A., Toomre J. *Ap. J.* 178:623
van Albada, T.S. 1982. *MNRAS* 201:939
van Albada, T.S. 1987. in *Structure and Dynamics of Elliptical Galaxies*, ed. P.T. de Zeeuw (Dordrecht: D. Reidel), p. 291
van Albada, T.S., Sanders, R.H. 1982. *MNRAS* 201:303
White, S.D.M. 1979. *MNRAS* 189:831
White, S.D.M. 1983. In *Internal Kinematics and Dynamics of Galaxies*, ed. E. Athanassoula (Dordrecht: D. Reidel), p. 337
Wright, G.S., James, P.A., Joseph, R.D., McLean, I.S. 1990. *Nature* 344:417

https://doi.org/10.1017/S0074180900244562 Published online by Cambridge University Press